Received: 1 January 2023 | Revised: 22 March 2023 | Accepted: 24 March 2023

DOI: 10.1002/pro.4633

FULL-LENGTH PAPER

THE PROTEIN SOCIETY WILEY

FRETing about the details: Case studies in the use of a genetically encoded fluorescent amino acid for distance-dependent energy transfer

Michael B. Cory[1] | Chloe M. Jones[1] | Kyle D. Shaffer[2] | Yarra Venkatesh[2] | Sam Giannakoulias[2] | Ryann M. Perez[2] | Marshall G. Lougee[2] | Eshe Hummingbird[2] | Vinayak V. Pagar[2] | Christina M. Hurley[1] | Allen Li[2] | Robert H. Mach[3] | Rahul M. Kohli[4,5] | E. James Petersson[2,4]

[1]Graduate Group in Biochemistry and Biophysics, Perelman School of Medicine, University of Pennsylvania, Philadelphia, Pennsylvania, 19104, USA

[2]Department of Chemistry, School of Arts and Sciences, University of Pennsylvania, Philadelphia, Pennsylvania, 19104, USA

[3]Department of Radiology, Perelman School of Medicine, University of Pennsylvania, Philadelphia, Pennsylvania, 19104, USA

[4]Department of Biochemistry and Biophysics, Perelman School of Medicine, University of Pennsylvania, Philadelphia, Pennsylvania, 19104, USA

[5]Department of Medicine, Perelman School of Medicine, University of Pennsylvania, Philadelphia, Pennsylvania, 19104, USA

Correspondence
E. James Petersson, Department of Chemistry, School of Arts and Sciences, University of Pennsylvania, Philadelphia, Pennsylvania 19104, United States.
Email: ejpetersson@sas.upenn.edu

Funding information
National Institutes of Health, Grant/Award Numbers: R01-GM127593, R01-NS103873, S10-OD030460, T32-AG000255, T32-GM071399, T32-GM133398, U19-NS110456; National Science Foundation, Grant/Award Numbers: CHE-1827457, DGE-1845298

Review Editor: John Kuriyan

Abstract

Förster resonance energy transfer (FRET) is a valuable method for monitoring protein conformation and biomolecular interactions. Intrinsically fluorescent amino acids that can be genetically encoded, such as acridonylalanine (Acd), are particularly useful for FRET studies. However, quantitative interpretation of FRET data to derive distance information requires careful use of controls and consideration of photophysical effects. Here we present two case studies illustrating how Acd can be used in FRET experiments to study small molecule induced conformational changes and multicomponent biomolecular complexes.

KEYWORDS
alphasynuclein, energy transfer, fluorescence, LexA, non-canonical amino acid

1 | INTRODUCTION

The fluorescent labeling of proteins has tremendous value for in vitro biochemical and biophysical experiments as well as cell-based imaging. These experiments can involve the use of a single chromophore to follow protein folding and binding, or the use of two chromophores to probe distances in protein complexes with Förster resonance energy transfer (FRET) (Lakowicz, 2006). In all of these experiments, incorporation of intrinsically fluorescent non-canonical amino acids (ncAAs) via Genetic Code Expansion (GCE) can provide significant advantages over labeling using fluorescent protein fusions or chemical modification methods (Cheng et al., 2020). Fusions to protein tags such as green fluorescent protein (GFP), SNAP tag, or Halo tag can introduce significant perturbations to the protein of interest and typically can only be fused to the N- or C-terminus of the protein, limiting their use in monitoring conformational

Michael B. Cory and Chloe M. Jones contributed equally to this study.

changes through FRET (Speight et al., 2014). Chemical labeling can be highly specific for a particular site on the protein surface, either through reaction with a single non-native cysteine residue or by reaction of an ncAA with a bioorthogonal functional group (Haney et al., 2015; Sletten & Bertozzi, 2009). However, both labeling approaches are restricted either to surface sites or proteins that can be efficiently unfolded and refolded after labeling. In contrast, intrinsically fluorescent ncAAs can be placed on the interior of a protein during biosynthesis, provided that they are positioned so as not to disrupt protein folding. This approach allows one to place at least one FRET label much more precisely to measure distance changes for a particular protein segment associated with protein folding or binding.

Here, we describe two case studies using the fluorescent amino acid acridonylalanine (Acd or δ), which can be incorporated into proteins in both bacterial and mammalian cells via GCE (Jones et al., 2021; Slilaty & Little, 1987). The first case study uses Acd in fluorescence polarization (FP) and FRET experiments to investigate the fibrillar aggregation of the protein α-synuclein (αS), which plays a central role in Parkinson's disease (Schulz-Schaeffer, 2010), and the effect of small molecules on fibril stability and conformation. The second case involves using Acd FP and FRET to study the mechanism of activation of the LexA transcriptional repressor by RecA, a trigger of bacterial hypermutation that can promote antibiotic resistance (Culyba et al., 2015). In both studies, we describe the rationale for the experimental design and the care taken to ensure that Acd incorporation does not disturb the protein's function. We also describe the thoughtful inclusion of control experiments necessary for quantitative interpretation of distance measurements through FRET. In order to keep our discourse here relatively concise, we focus on the particular aspects of these experiments that pertain to deriving distance information from FRET in complex systems. We refer the reader to previous publications with explicit protocols for incorporation of Acd and step-by-step instructions for FRET data fitting (Jones et al., 2020) as well as use of Acd in FP experiments (Cory et al., 2022a), in addition to Lakowicz's classic text on the basic principles of FP and FRET (Lakowicz, 2006). These studies should provide a useful guide to scientists wishing to use Acd for studies of protein structure, function, and dynamics.

1.1 | Types of fluorescence experiments PET

Before discussion of our choices of fluorescent probes, it is beneficial to briefly introduce FP and FRET in the context of other fluorescence experiments. FP is a technique that takes advantage of the intrinsic dipole moment of fluorophores, and the resulting anisotropy of emitted light. In particular, the polarization of a fluorescent molecule is inversely related to its rotational correlation time, as detailed below, so that observing a change in FP or anisotropy can provide information about changes in the size and shape of a molecule (Lakowicz, 2006). Therefore, FP is a useful technique for measuring molecular interactions between molecules of different sizes in which the fluorescent label is put on the smaller molecule so that an increase in FP/anisotropy occurs upon binding to the larger molecule, such as when a fluorescent small molecule or peptide ligand binds to a protein, or when a smaller protein binds to a larger protein (Figure 1) (Park & Raines, 2004; Rossi & Taylor, 2011). FP has also been used to measure changes in tumbling resulting from environments of different viscosities (Kuimova, 2012), changes in enzymatic function (Kitada et al., 2003), and formation of nucleic acid secondary and tertiary structure (Chen et al., 1999).

FRET is a non-radiative process of energy transfer between two chromophores with spectral overlap through dipole–dipole coupling and an a R^6 dependence, making it sensitive to changes in distance between donor and acceptor molecules (Lakowicz, 2006). Like FP, FRET can be used to monitor biomolecular interactions (Figure 1). The two methods have various advantages and disadvantages. While FP only requires labeling of one molecule and FRET requires that both molecules be labeled, FRET works well regardless of their relative sizes, whereas FP works best when the labeled molecule is significantly smaller than its partner. Additionally, if both labels are attached to the same molecule, FRET can be used to measure distance changes resulting from folding or conformational change in biomacromolecules (Figure 1). FRET has been applied to study binding and conformational change at the ensemble and single molecule levels, both in vitro and in living cells. (Haas, 2005; Schuler & Eaton, 2008; VanEngelenburg & Palmer, 2008). For both FRET and FP, environmental effects that alter the fluorophores' excitation or emission spectra (λ), molar extinction coefficients (ε), or quantum yields (ϕ) can complicate data interpretation and must be addressed, as we describe in our two case studies.

1.2 | Acd properties

Acd is a small (222 $Å^3$), uncharged fluorescent amino acid with properties that are well suited for studying proteins (Figure 1) (Speight et al., 2013). It has a high quantum yield (ranging from 0.98 in buffer to ~0.3 in hydrophobic protein pockets) and is more photostable than the other genetically incorporable fluorophores,

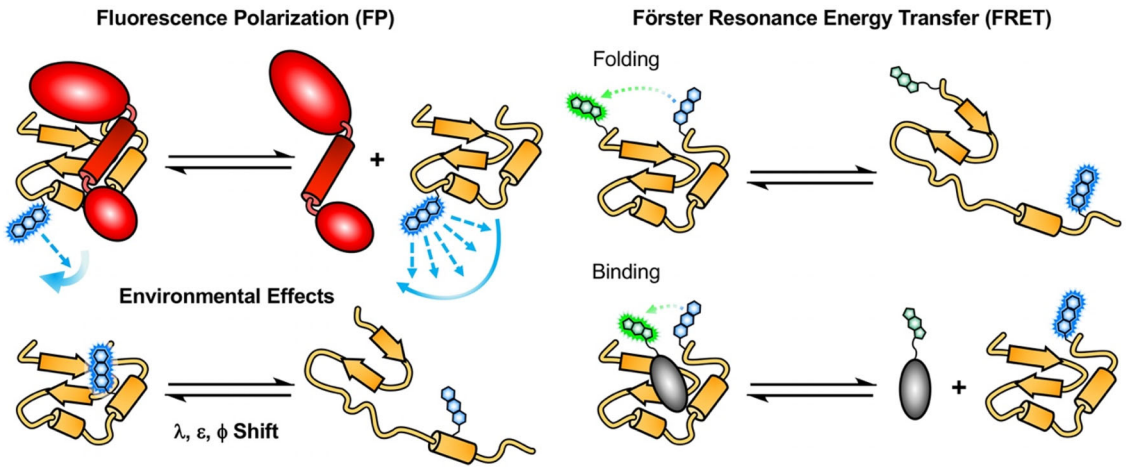

FIGURE 1 Fluorescence assays enabled by Acd. FP can be used to measure the effective size of biomolecular complexes with a label on one protein partner, where larger complexes will tumble slower and have higher FP. FRET can be used to measure either protein folding or binding equilibria, and time-resolved FRET can be used to measure kinetics. Environmental effects can alter chromophore properties to report on conformational changes, but can also complicate FP or FRET assays.

hydroxycoumarin ethylglycine, coumarinyl lysine, dansylalanine, and acetylnaphthalenylaminoalanine. Extensive photophysical characterization of Acd and comparison to other fluorescent ncAAs has been published previously (Jones et al., 2021). Additionally, Acd has a long fluorescence lifetime of 8–14 ns, which makes it useful for lifetime-based FRET measurements where one can resolve multiple populations in an ensemble (Jones et al., 2021). Together, changes in Acd's brightness and fluorescence lifetime can provide real-time information on its solvation environment, which in turn can be used to study protein folding/unfolding in a domain-specific manner. However, it must be noted that these environmental changes can become confounding factors for quantitative FRET interpretation and must be addressed using control experiments.

Acd's properties are also advantageous in FP or anisotropy studies. These measurements depend on the fluorophore's rotational correlation time and provide information on the fluorophore's molecular orientation and mobility, which can be used to monitor protein binding and cleavage events (Park & Raines, 2004). The anisotropy of a protein or complex is described for globular proteins by the Perrin equation:

$$r = \frac{r_0}{1 + \tau/\theta}$$

where r is the fluorescence anisotropy, r_0 is the fundamental anisotropy of the fluorescent dye, τ is the fluorescence lifetime of the dye, and θ is the rotational correlation time of the labeled molecule in question (Lakowicz, 2006). A similar equation describes an inverse relationship between FP and τ. As one can see, Acd's long fluorescence lifetime allows for greater sensitivity in studying protein interactions. Since FP and anisotropy depend inversely on fluorescence lifetime, longer lifetime fluorophores have a shallower change in FP as a function of apparent molecular weight, allowing one to distinguish differently sized complexes more easily (Hostetler et al., 2020).

With an additional partner chromophore, Acd can be used in distance-dependent energy transfer experiments involving nonradiative transfer of energy from a donor fluorophore to a nearby acceptor chromophore through space (Lakowicz, 2006). FRET is the most commonly employed mechanism in which the efficiency of energy transfer (E_{FRET}) is given by the following equation:

$$E_{\mathrm{FRET}} = \frac{1}{1 + \left(\frac{R}{R_0}\right)^6}$$

where R is the distance between the fluorophores and R_0 is the Förster distance of the specific donor/acceptor pair, which is determined by several characteristics of the system according to the following equation:

$$R_0^6 = \frac{9000(\ln 10)\kappa^2 \phi_{\mathrm{D}} J}{128\pi^5 n^4 N_{\mathrm{A}}}$$

where κ^2 is a geometric factor that relates the orientation of the donor and acceptor transition moments, ϕ_{D} is the quantum yield of the donor, n is the index of refraction of the interchromophore medium, N_{A} is Avogadro's

number, and J is the spectral overlap integral. J is formally defined as:

$$J = \int_0^\infty f_D(\lambda)\varepsilon_A(\lambda)\lambda^4 d\lambda$$

where $\varepsilon_A(\lambda)$ is the molar extinction coefficient of the acceptor at each wavelength λ and $f_D(\lambda)$ is the normalized donor emission spectrum given by:

$$f_D(\lambda) = \frac{F_D(\lambda)}{\int_0^\infty F_D(\lambda)d\lambda}$$

where $F_D(\lambda)$ is the fluorescence of the donor at each wavelength λ (Wu & Brand, 1994). While we will not discuss the photophysics of FRET at length, it is important to consider the factors that influence FRET when designing experiments. FRET is often referred to as a molecular "ruler", but extracting distance information from E_{FRET} measurements requires accurate calculation of R_0 (Stryer & Haugland, 1967; Van Der Meer et al., 1994). Environmental effects on chromophore properties can potentially alter the spectral shape of donor emission and acceptor absorption as well as the molar extinction coefficient of the acceptor and quantum yield of the donor. Therefore, to accurately calculate J, one must obtain spectra for the donor and acceptor chromophores in the same context that one is measuring FRET and not simply use generic spectra for the probes. To accomplish this goal, one can generate constructs labeled with the donor only or acceptor only and subject them to the same conditions as the donor/acceptor FRET construct. Such donor- or acceptor-only controls also allow one to determine any changes in ϕ_D or ε_A, enabling an accurate calculation of R_0, which permits the highest possible accuracy in the determination of distances for studying conformational change. It must be acknowledged that there still remains some ambiguity in R_0 based on uncertainty in the κ^2 and n terms, which are very difficult to determine experimentally. It is generally assumed that $\kappa^2 = 2/3$, which is the case for freely rotating dipoles. A water-like value of 1.33 is often assumed for n, despite the fact that the interchromophore medium is likely to consist of protein. In spite of these issues, there is still significant value in deriving distances from FRET measurements. In doing so, it is best to choose small chromophore pairs with R_0 values within useful ranges for measuring protein folding and conformational changes (Qiao et al., 2021).

1.3 | Acd applications

Acd has been widely used for FRET measurements, both as a donor and an acceptor fluorophore (Figure 2) (Speight et al., 2013; Ferrie et al., 2017; Haney et al., 2016). Short-range interactions have typically been probed with tryptophan (Trp) or methoxycoumarin (Mcm) as the donor and Acd as the acceptor. Mcm can be incorporated on the amino acid sidechain through solid phase peptide synthesis or through ligation of a peptide fragment to a larger protein (Tanaka et al., 2013). However, it is generally more practical to incorporate Mcm by reaction with a sidechain, as we have previously reported for a maleimide derivative that can be reacted with Cys to give C^{Mcm} (Ferrie et al., 2017; Jones et al., 2020). While use of Trp as a donor has the advantage that it can be genetically encoded, this usage is limited to cases where there are no essential Trp residues elsewhere in the protein. Trp also quenches Acd through photo-induced electron transfer (Speight et al., 2013) and this ability can convolute interpretation of FRET data. Mcm is our donor of choice because it is relatively environmentally insensitive and has a maximum absorption at a wavelength (325 nm) that coincides with a minimum in the Acd absorption spectrum, thereby avoiding undesired direct excitation of the Acd acceptor fluorophore. Boron dipyrromethene (BODIPY) is chosen as an Acd acceptor for similar reasons. The relatively narrow excitation spectrum of BODIPY does not have a significant tail in the 400 nm region (unlike fluorescein, for example) which minimizes direct BODIPY excitation when irradiating the Acd donor (Speight et al., 2013). Recently, Acd has also been studied as fluorescent donor in a distance-dependent quenching mechanism in proximity to a non-emissive metal using transition metal FRET (TM-FRET), particularly copper 1,4,7,10-tetraazacyclododecane (TETAC) chelates (Zagotta et al., 2021). BODIPY and Cu TETAC can be selectively conjugated to cysteine as C^{Bdp} and C^{CuT}, respectively. Additionally, when in close proximity to a lanthanide ion with appropriate spectral overlap of its f orbital transitions with Acd's emission spectrum, Acd can undergo energy transfer leading to lanthanide luminescence in a process referred to as luminescence resonance energy transfer (LRET) (Dadabhoy et al., 2002; Reynolds et al., 2008; Speight et al., 2013). LRET is mechanistically complex, with elements of FRET and Dexter transfer as well as photo-induced electron transfer (Bünzli & Eliseeva, 2011). Practically, LRET requires such short-range interactions that it is not very useful as a probe pair for distance measurement, but an Acd/Eu LRET pair can provide an enormous effective Stokes shift, with excitation of Acd at 385–400 nM and

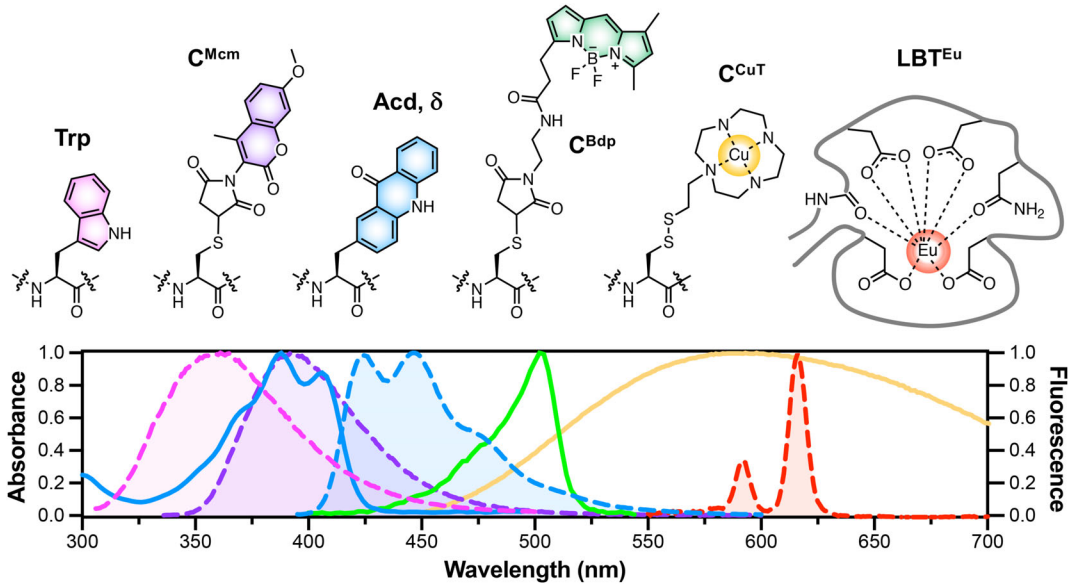

FIGURE 2 Acd FRET partners. (Top) Acd shown with energy donors, tryptophan (Trp) and cysteine conjugated methoxycoumarin (C^{Mcm}), and energy acceptors, cysteine conjugated BODIPY (C^{Bdp}), disulfide bound copper TETAC (C^{CuT}), and lanthanide binding tag peptide bound Eu (LBT^{Eu}). (Bottom) Absorption (solid lines) and emission (dashed lines, shaded) spectra of Acd FRET partners, colored like the structures above. All spectra are normalized to accentuate overlap with Acd spectra. Although LBT^{Eu} is an acceptor, the emission spectrum is shown to highlight the large effective Stokes shift from Acd sensitization.

emission of Eu at 645 nm (Figure 2). This type of LRET probe is often used as one of two partners in time-resolved FRET experiments, where an Acd/Eu donor could be combined with a red wavelength acceptor, taking advantage of the large effective Stokes shift and the delay in emission that comes from triplet transfer components in LRET to afford very low background FRET measurements. These time-resolved FRET experiments can be valuable for binding measurements where the probes are located on two different biomolecules, but the large probe sizes limit their use for studying protein conformation.

Each fluorophore/chromophore pair has a unique working range dependent on the type of energy transfer and the spectral overlap between the donor emission and the acceptor absorbance. Relevant spectra for all chromophores are shown normalized in Figure 2, and the full absorption and emission spectra of Acd and BODIPY are shown in Figure 4. Table 1 summarizes the properties of these Acd energy transfer pairs.

Here, we will focus on Acd/BODIPY FRET for a few reasons. Firstly, we have previously published on FRET studies with Trp, Mcm, and Cu-TETAC, including protocols for the synthesis and labeling of proteins with Mcm maleimide (Speight et al., 2013; Ferrie et al., 2017; Sungwienwong et al., 2018; Zagotta et al., 2021). We have even described Trp/Mcm/Acd three color FRET (Ferrie et al., 2017). As noted above, Acd sensitization of Eu emission has very limited utility in distance measurements, a goal in both of our case studies. Secondly, since BODIPY maleimide derivatives are commercially available and the Petersson laboratory makes Acd freely available in conjunction with the GCE4All Center at Oregon State University (22), Acd/BODIPY FRET should be easy for biochemists to implement without the need to synthesize custom reagents. Thirdly, we feel that the usable distance range of this FRET pair (Table 1) and visible wavelength excitation and emission make it an appealing choice for many users. Therefore, we will describe our two Acd/BODIPY case studies with some discussion of protein expression and labeling, but a primary focus on design of fluorescence experiments.

2 | RESULTS AND DISCUSSION

2.1 | Small molecule effects on α-synuclein fibril conformation

Our first case study involves the conformation of αS in fibrils. αS misfolding and aggregation have been linked to Parkinson's disease and related synucleinopathies, such as multiple system atrophy and Lewy body dementia (Koga et al., 2021). In its soluble form, αS is an intrinsically disordered protein that mediates neurotransmitter release by binding to synaptic vesicles (Benskey et al., 2016). Gene duplication, mutation, or cellular factors can trigger αS aggregation, leading to the formation of oligomers as well as amyloid-type fibrils (Mehra et al., 2019; Pancoe et al., 2022). The mechanism of αS misfolding is a highly active area of investigation with

TABLE 1 Acd chromophore pairs.

Chromophore pair	Excitation wavelength (nm)	Emission wavelength (nm)	Type of fluorescent interaction	R_0 (Å)	Working range (Å)[a]
Trp/Acd (Speight et al., 2013; Ferrie et al., 2017)	295	420	Acd acceptor	22.6	14–37
Mcm/Acd (Speight et al., 2013; Ferrie et al., 2017; Sungwienwong et al., 2018; Jones et al., 2020)	325	420	Acd acceptor	25.4	15–42
Acd/BODIPY (Speight et al., 2013)	386	511	Acd donor	49.4	30–80
Acd/Cu-TETAC (Zagotta et al., 2021)	386	420	Acd donor	14.9	9–24
Acd/Eu^{3+} (Reynolds et al., 2008; Speight et al., 2013)	386	615	LRET	<10	n/a

[a]Working range is defined as the distance range over which E_{FRET} goes from 0.95 to 0.05.

recent interest focusing on how aging-related changes in the cellular environment lead to aggregation and how pathology spreads between cells and between brain regions (Peelaerts et al., 2015; Peng et al., 2018; Marotta et al., 2021). Molecular probes that can be used to image the misfolding process in cells or in vivo represent one of the best tools for understanding the role of misfolding in Parkinson's disease etiology (Aliyan et al., 2019; Korat et al., 2021). To this end, the Petersson laboratory has worked in collaboration with the Mach laboratory and others to develop fluorescent and positron emission tomography (PET) imaging probes that bind with high affinity and selectivity to αS fibrils (Hsieh et al., 2018; Ferrie et al., 2020; Lengyel-Zhand et al., 2020). Additionally, molecules that bind to αS fibrils and cause their disaggregation have the potential to become Parkinson's disease therapeutics. We have also investigated such molecules (Haney et al., 2017; Daniels et al., 2019), and we wish to determine whether the small molecules being advanced as imaging probes cause changes to fibril structure and stability. If they do, it could limit their utility as imaging probes, but could motivate their use as new anti-aggregation leads. Here, we will demonstrate how αS labeled with Acd can be used to monitor the effects of small molecules on fibril stability through FP and their ability to induce conformational changes through FRET.

Before describing how to perform such experiments, it is worth considering what probes are best suited for studying fibril stability and folding. Although small molecule fibril binding fluorophores, such as thioflavin T, are commonly used to study protein disaggregation, using labeled proteins in FP assays has significant advantages, particularly avoiding false positives resulting from displacement of the dye rather than true disaggregation (Coelho-Cerqueira et al., 2014; Haney et al., 2017). However, given the sensitivity of αS to modification, labeling αS through N- or C-terminal fusion to GFP is not desirable as this approach has been shown to disrupt aggregation (Afitska et al., 2017). Even with small, synthetic fluorophores, one must take care to label the protein at sites that do not affect functional processes such as membrane binding, aggregation propensity, and native protein solubility (Haney et al., 2016). We chose our labeling sites based on literature data for mutations and post-translational modifications (PTMs) affecting αS aggregation, as well as prior data on labeling effects at each site (Pancoe et al., 2022). Labeling sites previously determined not to affect aggregation are shown in Figure 3. In

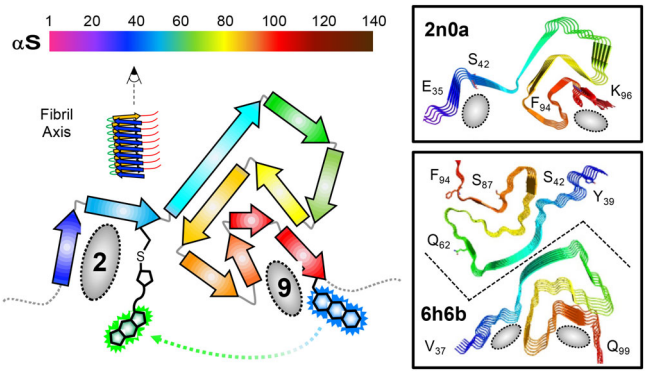

FIGURE 3 αS labeling sites. (Left) Cartoon of the fold of a single αS molecule in an in vitro fibril viewed down the fibril axis, colored according to the rainbow sequence scheme shown at top. Sites of Acd and C^{Bdp} labeling are indicated. (Right) Structures of αS fibrils from ssNMR (PDB ID: 2n0a) (Tuttle et al., 2016) and cryo-EM (PDB ID: 6h6b) (Guerrero-Ferreira et al., 2018) shown down the fibril axis. In 2n0a, the first and last residues, as well as positions 42 and 94 (shown in stick representation), are noted. In 6h6b, the first and last residues, as well as tolerated labeling positions (shown in stick representation), are noted. A dashed line is shown to clearly separate the two fibril strands.

this case, we chose positions 42 and 94 for labeling because they span the fibril core, which has been structurally characterized in a variety of solid-state NMR (ssNMR) and cryo-electron microscopy (cryo-EM) studies. The distance between Acd and C^{Bdp} is estimated to be ~50 Å in αS fibrils based on the single-stranded ssNMR structure (PDB ID: 2n0a) (Tuttle et al., 2016) and a representative double-stranded cryo-EM structure (PDB ID: 6h6b) (Guerrero-Ferreira et al., 2018). Therefore, the separation of these sites is in the middle of the working range for an Acd/BODIPY FRET pair, an ideal set up for monitoring conformational changes. Compounds from our PET imaging efforts have been demonstrated to bind to sites referred to as 2 and 9 in the fibril core through crosslinking mass spectrometry (MS) studies (Ferrie et al., 2020). In Figure 3, these sites are shown mapped onto the 2n0a and 6h6b structures. Given their locations, we expect that our 42/94 FRET pair will be sensitive to any conformational changes induced by the compounds. As one can see, we select our labeling sites through a combination of a holistic consideration of the protein structure and the expected distance range of any conformational dynamics. With the sites chosen, we move forward to expression and labeling of the αS constructs.

2.2 | α-Synuclein expression and labeling

Similar to our previously described methods for expression and double-labeling to produce Acd/Mcm labeled proteins (Ferrie et al., 2017; Jones et al., 2020), one can generate Acd/BODIPY proteins as shown for αS-$C^{Bdp}_{42}\delta_{94}$ in Figure 4. Cells are transformed with two plasmids, one encoding the Acd tRNA synthetase and complementary "amber suppressor" tRNA (Speight et al., 2013; Sungwienwong et al., 2017), and the other encoding the protein of interest with an "amber" (TAG) codon mutated at the site of Acd insertion (position 94) and a cysteine mutation at the BODIPY labeling site (Lakowicz, 2006). Our αS constructs also feature a C-terminal intein-His_6 tag for Ni column purification that can be tracelessly cleaved by treatment with β-mercaptoethanol (Batjargal et al., 2015). This purification tag is useful in cases where the ncAA is near the C-terminus and purification of full-length, ncAA-containing protein away from protein truncated at the TAG codon might otherwise be difficult. The intein-His_6 tag can be cleaved before or after reaction of the Cys residue with BODIPY maleimide (Bdp-Mal). Insertion of Acd and Bdp-Mal reaction with Cys are confirmed by MS. Typically, proteins are also purified by high-performance liquid chromatography (HPLC) and their purity confirmed by analytical HPLC and MS prior to use in fluorescence experiments. For FRET experiments, complementary donor-only (αS-δ_{94}) and acceptor-only (αS-C^{Bdp}_{42}) constructs must also be expressed and purified, using corresponding αS plasmids with only the TAG or Cys codons, respectively. MS characterization of all αS constructs is provided in Table S1, Figures S1, S2, S3, and S4. We note that for our BODIPY-labeled constructs, the C^{Bdp} conjugate has some absorbance in the 380–420 nm range of Acd absorbance (Figure 4); therefore, we excited Acd at 410 nm, where C^{Bdp} absorbance is minimal.

In order to assess the impact of labeling on aggregation, we perform aggregation experiments in which we monitor aggregation rates of the singly and doubly

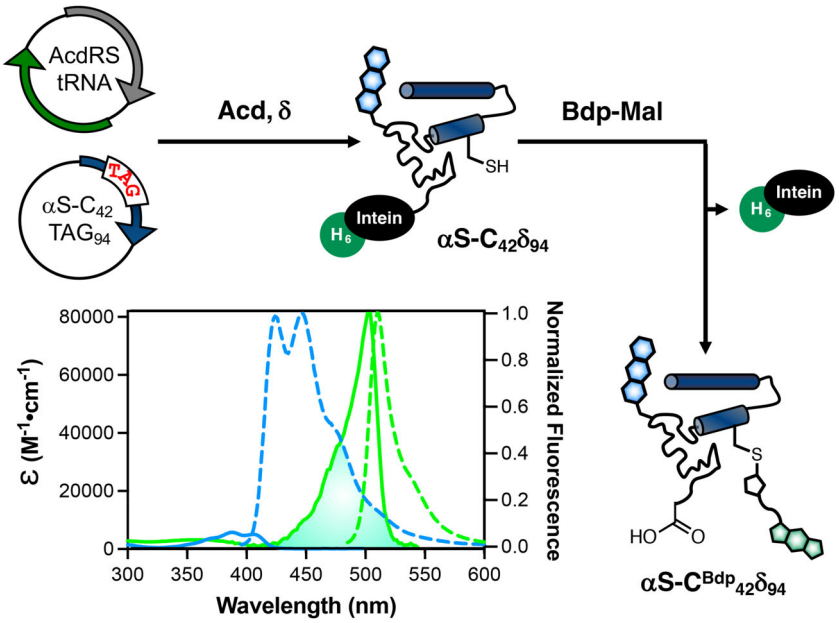

FIGURE 4 Expression and double-labeling of αS. *E. coli* cells are transformed with a plasmid for the AcdRS/tRNA pair and a plasmid for the protein (αS) with a Cys mutation at the site of BODIPY labeling and a TAG codon at the site of Acd labeling. The protein is expressed as a His_6-tagged intein fusion, purified, labeled with Bdp-Mal, the intein cleaved, and the protein further purified to give the Acd/C^{Bdp} double-labeled protein for FRET studies. (Inset) Acd (blue) and BODIPY (green) absorption (solid) and emission (dashed) spectra, highlighting the spectral overlap.

labeled constructs for comparison to wild type (WT) αS aggregation. Our fibrils are formed by aggregating a mixture of WT and labeled protein. The percentage of labeled protein varies with the brightness of the fluorophores and the application. For example, cellular imaging uses fibrils made with 25–100% labeled protein (Karpowicz Jr. et al., 2017; Marotta et al., 2021), whereas FP and intramolecular FRET studies of the type performed here are completed with 1–10% labeled protein (Haney et al., 2016, 2017; Haney & Petersson, 2018). There are several reasons why we do not use 100% labeled protein. Firstly, interactions between fluorophores on adjacent monomers in the fibril will confound both FP (due to homoFRET) and FRET (due to combinations of inter- and intramolecular FRET). Secondly, having 100% labeling increases the likelihood that the label disrupts protein folding and function. Thirdly, since labeled protein production is more labor intensive, using a lower percentage of labeled protein allows one to make more efficient use of resources. Here, we use 5% labeled protein to make it very unlikely that two labeled proteins are adjacent either within a single fibril strand or across the strands of two-stranded assembly. As noted above, we have previously incorporated a variety of fluorescent probes at positions 42 and 94 and confirmed that they do not substantially affect fibril aggregation rates or morphology (see Appendix S1, including Figure S8, for further discussion of αS labeling site validation) (Haney & Petersson, 2018).

2.3 | α-Synuclein FP assays

We began our assessment of whether some of the candidate PET probes altered fibril conformation upon binding. First, we wished to determine whether the molecules caused disaggregation of fibrils. For this test, an FP assay with αS-δ_{94} was deemed to be superior to a FRET assay since the FP signal is primarily influenced by the aggregation state of the protein (previous FP studies of disaggregation did show a positional dependence of FP signal, reflecting conformational dynamics, but monomer, oligomer, and fibril states were still discernable) (Haney et al., 2017). We tested VP-1-46 and BF-2846, two of our PET imaging leads, which bind to site 2 and site 9, respectively (Figures 3 and 5) (Ferrie et al., 2020; Lougee et al., 2022). It should be noted that although the compounds bind near the residues that we are fluorescently labeling, the labels are only present in 5% of the protein and are not expected to significantly interfere with compound binding. As positive controls, we used (−)-epigallocatechin gallate (EGCG), nordihydroguaiaretic acid (NDGA), and dopamine, three compounds known to cause fibril disaggregation (partial disaggregation in the case of dopamine) (Haney et al., 2017). As negative controls, we used treatment with DMSO vehicle and Ex-6, a compound shown to bind to αS fibrils but not disaggregate them (Ferrie et al., 2020). Upon 3 h incubation of our singly-labeled 5% αS-δ_{94} fibrils with these compounds, we saw a complete reversion of the FP signal to monomer values for EGCG and NDGA treatment, as well as a significant decrease for dopamine treatment, as expected (Figure 5). We saw no significant change in FP for Ex-6, VP-1-46, or BF-2846 treatment. These FP values were maintained after 24 h of incubation (Figure S9). We note that quenching of the dyes by the three compounds (observed in FRET experiments below) could inflate FP values somewhat, either by skewing the contribution toward the brighter fibrils or by reducing τ in the anisotropy equation. However, ~30% quenching would not be enough to alter the qualitative assessment that neither VP-1-46 nor BF-2846 seem to break up fibrils, similar to previously characterized compound Ex-6. This result supports the use of these three compounds in FRET measurements since, as noted above, FRET data would be difficult to interpret if disaggregation were occurring simultaneously.

2.4 | α-Synuclein FRET assays

For FRET measurements, we used three sets of fibrils formed from either 5% αS-C^{Bdp}_{42}, 5% αS-δ_{94}, or 5% αS-$C^{Bdp}_{42}\delta_{94}$ as respective donor-only, acceptor-only, and double-labeled constructs. First, we measured the emission spectra of each fibril construct in the absence of compound to determine whether E_{FRET} in the fibril state is consistent with the ssNMR and cryo-EM structures. Then, we incubated the three sets of fibrils with either Ex-6, VP-1-46, or BF-2846 for 24 h, reading spectra at 0, 1, and 24 h. As shown for all three cases in Figure 6, there is overall quenching of fluorescence upon addition of the compounds (Figure 6c), so changes in FRET must be interpreted carefully using donor-only and acceptor-only controls. When the αS-δ_{94} and αS-C^{Bdp}_{42} spectra are examined, one can see that both Acd and BODIPY fluorescence decrease in the presence of the small molecules (Figure 6a,b), either through environmental changes or precipitation of some fibrils. Regardless, when one compares the sum of the donor-only and acceptor-only spectra to the spectrum of the double-labeled protein, it is clear that there is a decrease in Acd emission and an increase in BODIPY emission, demonstrating a FRET interaction in untreated fibrils (Figure 6d) as well as fibrils treated with Ex-6 (Figure 6e), VP-1-46 (Figure S10), and BF-2846 (Figure S10).

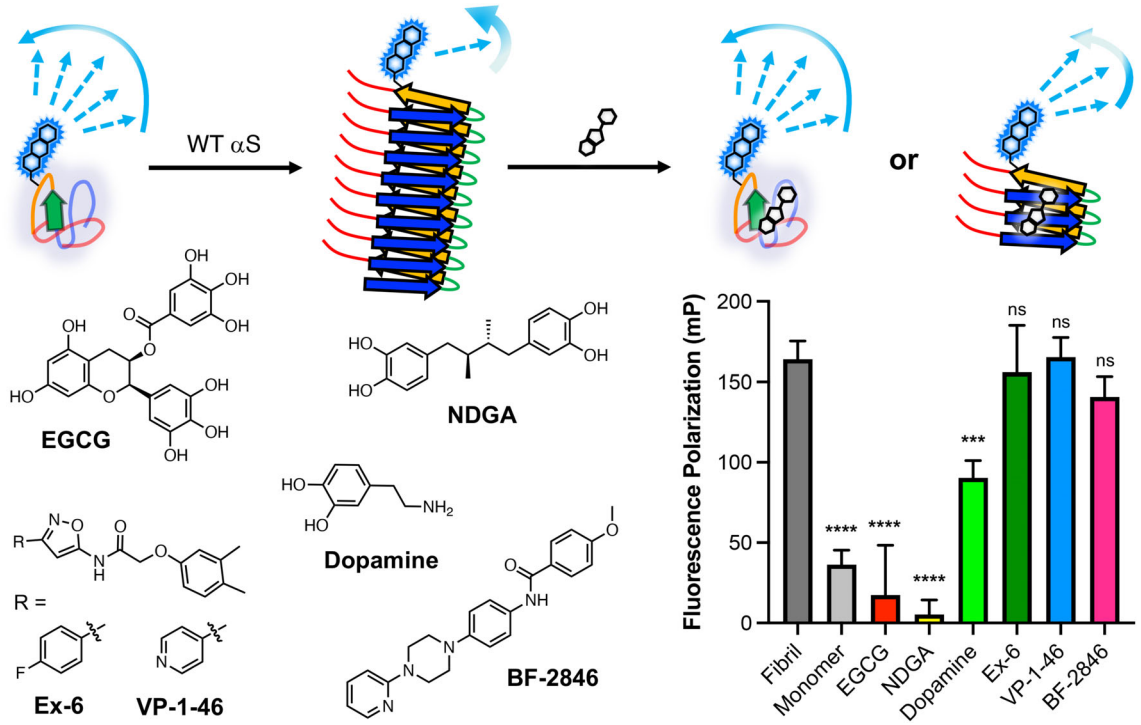

FIGURE 5 αS FP assay. Fibrils are made by aggregating 5% αS-δ_{94} with 95% WT αS, then FP is monitored while the 5% labeled fibrils are incubated with small molecules (with shaking at 25 rpm, 37°C). After 3 h, FP changes indicate reversion to small dynamic structures that are similar to monomers for positive controls EGCG and NDGA and correspond to a large oligomeric structure for dopamine. One-way ANOVA tests show significance of FP changes relative to untreated fibril: ****$p < 0.0001$; ***$p < 0.001$; ns, not significant.

To determine E_{FRET}, we then fit the αS-$C^{Bdp}{}_{42}\delta_{94}$ doubly-labeled spectra to a linear combination of the singly labeled spectra by adjusting the A and B parameters to minimize the square difference:

$$\sum_{\lambda}\left(I(\lambda)_{DA}-\left(AI(\lambda)_{D}+BI(\lambda)_{A}\right)\right)^{2}$$

where $I(\lambda)_{DA}$, $I(\lambda)_{D}$, and $I(\lambda)_{A}$ represent the fluorescence intensity at a given wavelength from double-labeled αS-$C^{Bdp}{}_{42}\delta_{94}$, donor-only αS-$\delta_{94}$, and acceptor-only αS-$C^{Bdp}{}_{42}$, respectively (Figure 6f). We note that determining E_{FRET} based on acceptor quenching in this manner is most useful in determining distances from E_{FRET} values, for reasons described in detail in Appendix S1. From this fit, E_{FRET} is then simply calculated as $1-A$. For untreated fibrils, we obtain an E_{FRET} value of 0.40. To properly estimate interchromophore distance from E_{FRET}, we must determine R_0 for Acd and BODIPY in this environment by comparing the emissions of the Acd-only construct and free Acd amino acid to determine the donor quantum yield ϕ_D. We find that Acd is quenched significantly, with ϕ_D decreasing from 0.95 for the free amino acid in water to 0.64 at position 94 in αS fibrils (Table S2). A fully rigorous determination of R_0 would also require determining the acceptor extinction coefficient, ϵ_A, and the spectral overlap integral, J, in the fibril environment. However, these values do not typically change with environment as much as ϕ_D and can be difficult to measure for dilute samples. Using the Φ_D correction, we determine an R_0 value of 46.3 Å, from which we calculate a distance R of 43 Å. This result is in reasonable agreement with the C_β-C_β distance for Ser_{42} and Phe_{94} of 39 Å or 49 Å observed in the 2n0a ssNMR and 6h6b cryo-EM structures, respectively. By performing the same fitting procedure for the fibril spectra in the presence of the compounds, we find that after 1 h, E_{FRET} decreases from 0.40 for untreated fibrils to 0.22, 0.17, and 0.29 for fibrils treated with Ex-6, VP-1-46, and BF-2846, respectively. After correcting for changes in the donor quantum yield ϕ_D (note Acd quenching upon addition of compounds in Figure 6), we determine that these changes in E_{FRET} correspond to increases in the average distance between residues 42 and 94 from 43 Å in untreated fibrils to 53 Å, 56 Å, and 50 Å in fibrils treated with Ex-6, VP-1-46, and BF-2846, respectively, for 1 h. These structural changes are generally maintained after 24 h, with BF-2846-bound fibrils having a more limited conformational change (Figure S10). FRET and distance data are summarized in Table 2. Experimental error is estimated based on the variance among the three replicate spectra which were averaged for each donor-only,

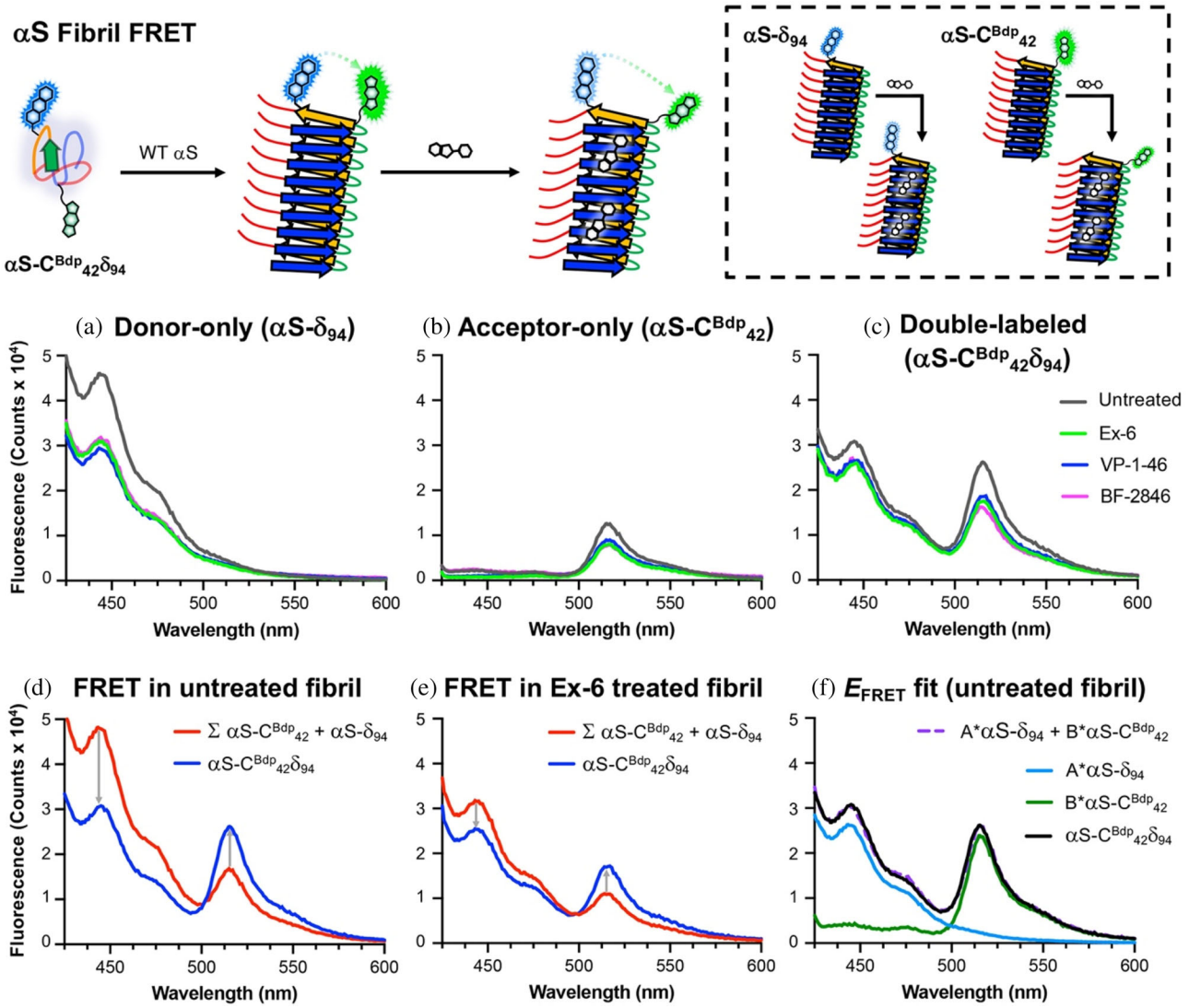

FIGURE 6 αS fibril FRET. (Top) Experimental scheme for making fibrils with 5% αS-$C^{Bdp}_{42}\delta_{94}$ and treating them with Ex-6, VP-1-46, or BF-2846. (Inset) Control experiments with fibrils made from 5% αS-C^{Bdp}_{42} or 5% αS-δ_{94}. Middle: Raw spectra for untreated fibrils (0 h) and fibrils treated for 1 h with Ex-6, VP-1-46, or BF-2846; (a) donor-only controls, (b) acceptor-only controls, (c) double-labeled fibrils. (Bottom) FRET analysis of (d) untreated fibrils and (e) Ex-6 treated fibrils showing a comparison of the double-labeled spectrum to the sum of donor-only and acceptor-only spectra. An example E_{FRET} calculation for untreated fibril data showing the weighted donor-only and acceptor-only spectra as well as their sum compared to the double-labeled spectrum.

acceptor-only and double-labeled spectrum used in the calculations. In Appendix S1, we have also included a discussion of the impact on R values of deviations from our assumptions regarding $\kappa^2 = 2/3$ and n (Figure S11 and Table S3).

While these initial experiments should be supported by additional studies with different fluorophore placements, variations in small molecule concentration, and alternate fibril preparations, they demonstrate that Ex-6, VP-1-46, and BF-2846 all induce conformational changes in αS fibrils upon binding and provide a hint that these changes are more limited for the Site 9 ligand, BF-2846. This information is valuable for the development of these compounds as PET imaging probes, where induced conformational changes can affect their dissociation rates. Furthermore, despite not disaggregating fibrils, the conformational changes may alter the toxicity of the fibrils or their ability to seed pathology in healthy neurons, both potential therapeutic avenues. This case study of a small molecule induced conformational change in αS amyloid fibrils shows how, with appropriate labeling strategies and control experiments, one can study an intramolecular rearrangement in a complex oligomeric system in spite of changes to both donor and acceptor fluorescence that are independent of the FRET interaction. Our second case study, also of an oligomeric complex, demands

TABLE 2 FRET efficiencies and interchromophore distances.

	Untreated	Ex-6 1 h	Ex-6 24 h	VP-1-46 1 h	VP-1-46 24 h	BF-2846 1 h	BF-2846 24 h
E_{FRET}	0.40	0.22	0.25	0.17	0.22	0.29	0.40
R (Å)	43	53	52	56	54	50	47

an even more sophisticated labeling strategy and series of control experiments.

2.5 | LexA, RecA, and the SOS response in bacteria

The SOS response is a generalized DNA damage response pathway in bacteria. SOS activation results not only in direct, high-fidelity repair of DNA damage, but also DNA damage tolerance, whereby DNA lesions are bypassed in a low-fidelity manner (Bell & Kowalczykowski, 2016; Maslowska et al., 2019). This bifunctionality makes the SOS response an attractive therapeutic target in the ongoing fight against antibiotic resistant microbial infections (Memar et al., 2020; Podlesek & Žgur Bertok, 2020). Activation of the SOS response is dictated by the formation of a ternary complex between single-stranded DNA (ssDNA) and the proteins RecA and LexA. LexA is a homodimeric repressor-protease that is comprised of an N-terminal DNA binding domain and C-terminal dimerization domain containing a serine protease catalytic core. RecA is the "sensor" of DNA damage. In an ATP-dependent process, RecA monomers form lengthy filaments along the ssDNA that accumulates during DNA damage. This nucleoprotein filament, termed RecA*, then binds to free LexA dimers, triggering a conformational change that initiates LexA autoproteolysis (Figure 7a) (Slilaty et al., 1986; Slilaty & Little, 1987; Little et al., 1994; Luo et al., 2001). The resulting depletion of LexA within the cell leads to a temporally-ordered upregulation of SOS response genes as bound LexA dimers dissociate from promoters (Culyba et al., 2018).

Although much is known about the formation of RecA* filaments, studying its interaction with LexA has remained challenging given the complexity of the LexA-RecA-ssDNA interaction. Several models exist in the literature for LexA binding to RecA*, each placing LexA into the helical groove of the filament. Two prevailing models differ greatly in the proposed binding orientation of LexA relative to RecA*, with the "side-on" and "CTD-bound" models differing in whether one of the monomers or both CTDs are engaged with RecA* (Figure 7a, inset) (Yu & Egelman, 1993; VanLoock et al., 2003; Adikesavan et al., 2011; Kovačič et al., 2013). In addition to open questions regarding the binding mode, the kinetics of RecA binding to LexA have been poorly understood, despite the fact that kinetics are key to temporal control over the SOS response. We recognized that Acd is well suited for use as a tool to address these key gaps in knowledge. To this end, we have used amber suppression as a means to co-translationally incorporate Acd at a target position, allowing us to achieve quantitative labeling and eliminate the need for complex purification with in vitro post-translational labeling. Because amber suppression typically negatively impacts protein yield, we decided to label LexA over RecA for these experiments because LexA generally expresses more favorably. Another advantage to Acd incorporation is the ease with which we were able to screen candidate positions in LexA for Acd tolerance, using the fraction of soluble protein as a metric (Figure 7b, left). Screening of a variety of positions, both on the basis of amino acid properties and evolutionary conservation, did not initially lead to any reliable predictors for Acd tolerance at a given position. However, a subsequent machine learning approach achieved successful prediction within LexA and RecA (Hostetler et al., 2018; Giannakoulias et al., 2021). The combination of empirical data and machine learning-enabled prediction give us confidence in our ability to choose Acd sites that are tolerated by the LexA structure; nevertheless, in order to be used in dissection of the SOS complex they must also be non-perturbing to LexA function.

2.6 | Previous LexA Acd studies

As noted above, the long fluorescence lifetime of Acd makes it a particularly effective probe for FP measurements, which report on a molecule's (or complex's) rotational mobility. This section details how we have used Acd previously to study the kinetics of SOS complex assembly. For complex assembly study by FP, we first needed to determine a suitable labeling location. To do so, we advanced a subset of well-tolerated Acd substitution candidates for LexA (LexA-δ_n, $n = 9$, 21, 36, 60, 86, 98, 105, 111, 130, 161, 166, 174, 186, 201) and tested if they were amenable to anisotropy-based measurements. Based on their Z-scores, we determined that LexA-δ_{161} was the optimal labeled construct for FP experiments (described in detail in Appendix S1). Depending on the

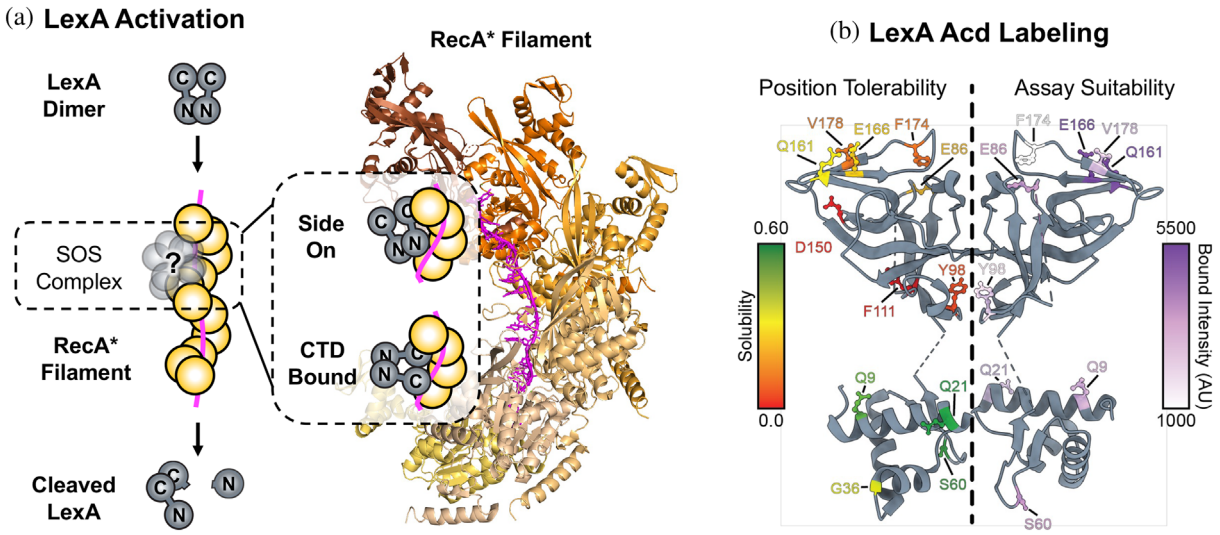

FIGURE 7 LexA activation and criteria for LexA labeling position. (a) LexA binding to RecA* filaments (formed by ≥3 RecA monomers, ssDNA, and ATP) induces a conformational change in LexA that triggers self-cleavage of at least one LexA monomer, leading to activation of the SOS response genes. The structure of RecA* (PDB ID: 3cmu) (Chen et al., 2008) is shown with different monomers in distinct colors and ssDNA in pink. (Inset) Two possible models for the LexA/RecA interaction in the SOS complex. (b) Analysis of Acd labeling sites in LexA mapped onto the LexA dimer structure (PDB ID: 1jhe) (Luo et al., 2001). Position tolerability is derived from the fraction of soluble protein determined for LexA-δ_n variants compared to WT LexA. Assay suitability is determined by comparing the fluorescence intensity of fixed concentrations of LexA-δ_n variants.

available instrumentation, FP can be used for either kinetic or endpoint equilibrium analysis of formed complexes, and in our LexA work we have relied upon both types of experiments. Using FP competition assays, we were also able to assess the affinity of a variety of unlabeled LexA variants. These prior results demonstrated that the N-terminal DNA-binding domain of LexA, which is lost after autoproteolysis, is not essential to RecA* binding. This insight helped to eliminate some candidate models for LexA-RecA* engagement, suggesting that a "side-on" model if correct would likely not include extensive contacts between the NTD and RecA* (Hostetler et al., 2020). Thus, exploiting the properties of Acd for FP enhanced our understanding of the kinetics of SOS complex assembly and offered some limited insights into LexA orientation relative to RecA*. In a subsequent study, we used the same FP assay in combination with genetic fusion of RecA monomers, forming concatenated multimers of 2–6 RecA subunits (Cory et al., 2022b). Measuring binding of LexA using Acd FP as well as other assays, we determined that three RecA subunits are sufficient to activate LexA. This result allowed us to refine our models of the SOS complex once again, narrowing down the number of RecA units that bind to LexA to 3. However, this information still only provided a very coarse-grained picture of the complex, and we recognized that there were additional opportunities for using Acd in FRET experiments to determine distance measurements which could be used for further refinement of the model.

2.7 | SOS complex Acd FRET

A working model for the LexA orientation when bound to RecA* would inform both in silico efforts to dock LexA onto the RecA* filament and could be informative for efforts to disrupt this interface with small molecule inhibitors. FRET can be used as a "molecular ruler," allowing for inter- and intramolecular distance determination, to build a low-resolution structural model of LexA binding to RecA*. One additional advantage Acd has in a FRET system is that because the fluorophore moiety is directly linked to the protein backbone, there is much less positional uncertainty in relating FRET-derived distances to protein conformation. In this section, we will discuss the optimizations required for setting up a working FRET system with Acd, including selection of a FRET partner and system-specific controls.

In choosing a construct for FRET experiments, we considered the same set of well-tolerated Acd substitution candidates for LexA and examined the Acd intensity with free LexA as well as in the SOS complex. For FRET experiments, we wanted to use the brightest possible Acd construct and one with little or no change in fluorescence

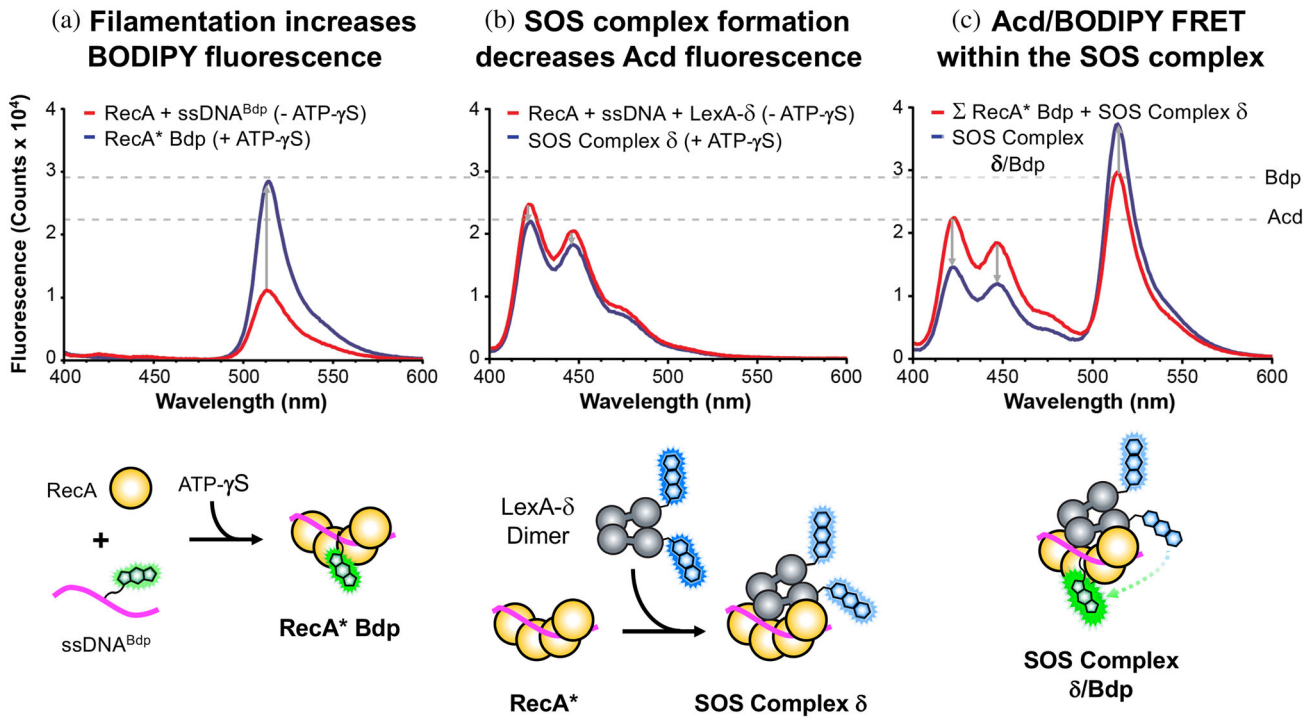

FIGURE 8 SOS complex FRET experiments. Control experiments in which BODIPY labeled ssDNA^{Bdp} is incubated with RecA with ATP-γS to form RecA* Bdp (a) or Acd-labeled LexA-δ is incubated with RecA and unlabeled ssDNA with ATP-γS to form SOS complex δ (b) are compared to corresponding experiments without ATP-γS. These control experiments allow us to identify a small decrease in Acd emission (b) and a large increase in BODIPY emission (a) to permit proper interpretation of FRET in the SOS complex δ/Bdp where both labeled components are present (c) by comparison to the sum of emission spectra from RecA* Bdp and SOS complex δ.

in the SOS complex, as such changes could confound interpretation of FRET data. Once again, LexA-δ_{161} proved to be the most suitable construct (Figure 7b, right). It was the brightest and experienced the smallest changes in fluorescence upon formation of the SOS complex. Based on all of these studies, we chose LexA-δ_{161} for FRET experiments, and we hereafter refer to this construct simply as LexA-δ.

With the Acd position in LexA already determined, we needed to decide on (1) whether the FRET partner for Acd would be installed on RecA or within the ssDNA and (2) the specific fluorophore that would serve as either FRET donor or acceptor to Acd. Because a FRET probe installed on RecA would be present on every RecA unit within the filament and would require several upfront optimizations, we reasoned that it was preferable to instead introduce the probe on the ssDNA. To this end, we used a synthetic oligo containing a 5-octadiynyl dU nucleotide as the central base, whereby the terminal alkyne could allow for flexible labeling with a fluorophore of choice. By positioning the label in the central region of the ssDNA, we reasoned that it should be ultimately situated in the groove of the filament where LexA is presumed to bind (Figure 7). Also, by choosing an appropriate length of ssDNA, we could control how many RecA subunits were bound. In this case, a 13mer ssDNA is expected to bind 4 RecA subunits (Rajan et al., 2006), limiting the assembled complex to a single LexA binding site as determined in our FP experiments described above (Figure 8). Although we have shown that it is possible for LexA to bind to filaments of only three RecA subunits, the affinity of ssDNA for the RecA 3mer is 5-fold lower compared to the RecA 4mer (Cory et al., 2022b). Therefore, we designed our experiments to target a RecA 4mer using the 13mer ssDNA in order to maximize formation of the ternary SOS complex, as discussed in more detail below.

As candidate fluorophores, we considered either methoxycoumarin or BODIPY which, as discussed above, can serve as either a donor or acceptor for Acd, respectively. We decided to use BODIPY labeled ssDNA (ssDNA^{Bdp}) for a few reasons. We were concerned that methoxycoumarin FRET signals might be difficult to interpret owing to the significant overlap of its emission with Acd's emission. While C^{Mcm}/Acd FRET pairs have been useful to us in the past, given the uncertainty in our models of the SOS complex and the possibility of FRET with two Acd probes (each on one LexA monomer), we wished to minimize any added complexity in this situation. Also, the working distance for Mcm/Acd FRET is

limited by the short (25 Å) Förster distance compared to the longer Förster distance (49 Å) for Acd/Bdp (Speight et al., 2013). Crude modeling of the SOS complex indicated that many potential LexA orientations would place the Acd probes outside the useful FRET range for Mcm (20–40 Å). Therefore, the Acd/Bdp FRET range (35–70 Å) was better suited to initial investigations since there was a higher likelihood of a positive FRET signal. For these reasons, we decided to advance ssDNA^{Bdp} as the candidate for FRET pairing to LexA-δ. It was synthesized from a commercial custom-synthesized oligonucleotide and a BODIPY azide derivative, then purified by HPLC and its identity confirmed by MS (Figures S5 and S6). Before proceeding with FRET experiments, we first tested whether the fluorescent label and spacer arm impacted the ability of the SOS complex to form, using RecA-stimulated LexA proteolysis as a proxy (Figure S7). A comparison to an unlabeled GGT 13mer oligo shows that the Bdp label did not negatively affect the cleavage of LexA by RecA, indicating that the SOS complex was able to form in vitro. Thus, we successfully identified labeling positions in both LexA and RecA* that do not affect function. Next, we evaluated the baseline signals of the labeled SOS complex components.

Accurate quantification of FRET relationships requires optimization and consideration of several parameters, such as changes to the emission properties of the two chromophores upon conformational change and the population of different states. In many intermolecular FRET experiments, one needs to consider the contributions from the free donor and acceptor labeled components (LexA-δ and ssDNA^{Bdp}). For the SOS complex, we must also consider unlabeled components (RecA and ATP) required for ternary complex formation. We wished to have the concentration of each constituent such that we maximized complex formation and simultaneously minimized free constituents, all while remaining within working signal range for the detector. These considerations are especially important in a case where the brightness of the two dyes being used is not equivalent—Acd's brightness is 1/10 that of BODIPY. Using the K_d values of the components determined in our previous experiments, we were able to consider the effects of concentration variation on the speciation of the components to find conditions that maximized formation of the SOS FRET complex, while simultaneously minimizing free components (see Figure S12, Table S4 and discussion in Appendix S1).

Another set of considerations for our FRET experiment design is related to the environment-dependent effects on both Acd and BODIPY. In hydrophobic environments, the observed fluorescence of Acd decreases while the observed fluorescence of BODIPY increases. The opposing direction of these changes could lead to the artifactual appearance of FRET. To control for this possibility, we prepared reaction mixtures containing one of the constituents (either donor or acceptor) in conditions that either prevented complex formation (minus ATP-γS, used as a hydrolytically stable ATP analog) or allowed for complex formation (plus ATP-γS) and monitored the effects of complex formation on each fluorophore independently before exploring the two components together. Indeed, we see a large increase in BODIPY fluorescence under complex-forming conditions (Figure 8a), whereas we only see a modest decrease in Acd fluorescence under complex-forming conditions (Figure 8b). Note that due to differences in the BODIPY probe and light scattering resulting from the semi-solubility of αS fibrils, the background signal in the 400–500 nm range is lower for ssDNA^{Bdp} than for αS-C$^{Bdp}_{42}$ from the previous case study. Establishing these baseline effects is critical to the quantitative evaluation of FRET for distance determination. In the key experiment, when the two labeled components are mixed, we see a further increase in BODIPY fluorescence paired with a further decrease in Acd fluorescence (Figure 8c). The coupled changes, in comparison to our careful control experiments, convincingly demonstrate FRET and offer clear evidence of LexA-δ engagement within a reasonable distance to permit energy transfer to the modified nucleobase deep within the RecA* groove. However, there are still some additional issues that must be resolved to begin modeling based on FRET distances.

The most significant remaining ambiguity is that LexA is a dimer, so the functional LexA-δ unit binding in the SOS complex contains two Acd residues, at the 161 positions in the respective monomers. In Figure 8, we have depicted this as a simplified case in which LexA binds to RecA* in a side-on fashion, with only one Acd sidechain transferring energy to the BODIPY acceptor. If that were the case, the 36% decrease in total Acd emission would correspond to E_{FRET} of 0.72 for the nearer Acd with E_{FRET} of 0 for the farther Acd (E_{FRET} determined by fitting the SOS complex δ/Bdp double-labeled spectrum to a linear combination of the SOS complex δ donor and RecA* Bdp acceptor spectra, see Figure S13). We note that the value of 0.36 comes from simply taking the arithmetic mean of $E_{FRET} = 0.72$ and $E_{FRET} = 0$, which assumes that the two Acd donors interact independently with the BODIPY acceptor (see Appendix S1 for justification of this assumption). Our E_{FRET} of 0.72, assumed to derive entirely from transfer by the nearer Acd, provides a distance estimate of 36 Å between Acd and BODIPY in the SOS complex δ/Bdp (R determined using $\Phi_D = 0.36$, corrected for Acd quenching in the SOS complex, as described above for αS FRET). If LexA

indeed binds to RecA in a side-on fashion, a model supported by prior low resolution cryo-EM data and the fact that only one LexA subunit is cleaved at a time in the SOS 5-octadiynyl dU complex (Giese et al., 2008; Butala et al., 2011), then the >60 Å distance between Q_{161} positions in the two monomer units would dictate that one Acd residue has only a minimal FRET interaction with the BODIPY in ssDNA^{Bdp}. However, it is of course possible that the observed E_{FRET} is a result of a more complex scenario with FRET interactions occurring for both Acd donors (some potential models for the SOS complex are shown in Figure S14). It also must be acknowledged that we are working under the common assumption that the dyes are freely rotating, so the κ^2 orientational parameter in the FRET equation is set to 2/3. While this assumption is still largely valid as long as there is some conformational flexibility for the chromophores (as we have shown with thioamide FRET probes) (Yoon et al., 2020), distance interpretations change if κ^2 deviates significantly from 2/3, as is the case for highly restricted chromophores.

During the review of this manuscript, a cryo-EM structure (PDB ID: 8gms) of truncated LexA bound to RecA* has been reported (Gao et al., 2023). Although lacking the NTD of LexA, the structure suggests that the 'side-on' model of binding is correct, with resulting distance measurements that would be highly consistent with our observations if a single Acd is involved in energy transfer with BODIPY (Figure S15). Since the exact register of our ssDNA^{Bdp} in the RecA binding pocket cannot easily be related to the RecA-bound DNA in cryo-EM structure, we computed the distance from the Q_{161} γ-carbon to the thymine methyl carbon for all six bases in the 8gms structure. The average distance for the nearer LexA protomer is 34 ± 7 Å and the average distance for the farther LexA protomer is 61 ± 2 Å, in remarkable agreement with our side-on FRET model having respective distances of 36 Å and >60 Å. In future studies, a series of FRET experiments with different LexA-δ_n and ssDNA^{Bdp} constructs should allow us to further discriminate the relative orientation of LexA and RecA*. For example, time-resolved FRET measurements can be used to address questions of dynamics that are not accessible through cryo-EM. Using the system we have described, other well-tolerated and bright Acd positions such as 86, 166, and 201 or selecting other ssDNA labeling positions like the 5′ and 3′ ends could provide added distance constraints for modeling of full-length LexA binding. Thus, with this functioning LexA/RecA FRET system in place, the door is now open for future systematic interrogations to gain a better understanding of the orientation of LexA binding to the RecA* filament, potentially identifying the molecular mechanism by which LexA cleavage is induced.

3 | CONCLUSIONS

We have used two case studies to illustrate how FRET can be used to quantitatively estimate intra- and intermolecular distances in multi-component oligomeric complexes by properly employing control constructs and designing labeling schemes to restrict the FRET interactions to certain scenarios. In the first case study, we used 5% labeling to ensure that we would only observe intramolecular FRET in our αS constructs. Careful use of donor-only and acceptor-only controls allowed us to correct for quenching of both Acd and BODIPY due to the addition of the small molecules, altering E_{FRET} calculations and changing ϕ_D, which alters R_0 and ultimately the estimation of the intrachromophore distance, R. As noted above, these controls still neglected changes in R_0 due to altered acceptor extinction coefficient, ε_A, and spectral overlap integral, J. However, the shapes of the Acd emission spectrum and BODIPY absorption spectrum do not change much with environment, nor does the BODIPY extinction coefficient, so these are reasonable simplifications. The second case study presented an even more challenging scenario in which LexA, RecA, and ssDNA component concentrations needed to be carefully chosen to drive complex formation and minimize the concentrations of free Acd-labeled LexA, RecA, and BODIPY-labeled ssDNA. Again, careful controls in which we formed SOS complexes where one labeled component was substituted allowed us determine baseline Acd and BODIPY emission from which E_{FRET} could be properly calculated. The concurrent publication of the LexA/RecA cryo-EM structure (Gao et al., 2023) provided an ideal "blinded" test of the accuracy of our FRET measurement. We hope that the approaches used in our two case studies provide the reader with guidance on how to apply similar strategies to biomolecular FRET experiments of their own.

4 | METHODS

4.1 | Protein production

Expression, purification, and Acd and/or BODIPY labeling of αS were done essentially as described for Acd and Mcm labeling in Jones et al. (2020), with Bdp-Mal substituted for Mcm-Mal. Detailed procedures and product characterization by MALDI MS are provided in Appendix S1. Expression and purification of both RecA

and Acd-labeled LexA was done as previously described (Hostetler et al., 2018, 2020; Cory et al., 2022a).

4.2 | αS fibril preparation

Protein construct concentrations were determined by absorption spectroscopy (WT αS: $\varepsilon_{280} = 5120\ M^{-1}\ cm^{-1}$, αS-$\delta_{94}$: $\varepsilon_{386} = 5700\ M^{-1}\ cm^{-1}$, αS-$C^{Bdp}{}_{42}$ and αS-$C^{Bdp}{}_{42}\delta_{94}$: $\varepsilon_{503} = 82{,}000\ M^{-1}\ cm^{-1}$)[1]. Labeled αS monomer was combined with WT αS to a final concentration of 100 μM and 95:5 unlabeled to labeled construct. The tubes were sealed with Teflon tape and Parafilm and incubated at 37°C with shaking at 1300 rpm for 3–5 days.

4.3 | αS FP experiments

The αS-δ_{94} fibrils were diluted to a final concentration of 10 μM (relative to monomeric αS) in 1× PBS buffer and pipetted in triplicate into a nonsterile Greiner black, flat μClear, 96 well half area microplate (Cat. #675096) to a final volume of 100 μL. Additionally, Acd amino acid and αS-δ_{94} monomer were diluted to 0.5 μM (matching the Acd concentration in 10 μM 5% αS-δ_{94} fibrils) to act as controls. All small molecules were solubilized in DMSO to a concentration of 10 mM. Prior to small molecule addition, starting polarization values were obtained and the gain and Z-position optimized on a Tecan SPARK plate reader using $\lambda_{ex} = 385 \pm 5$ nm. Small molecules were then added to a final concentration of 100 μM to their respective wells. FP measurements were acquired at 3 and 24 h after small molecule addition with the plate incubated at 37°C between measurements with shaking at 500 rpm.

4.4 | αS FRET experiments

αS-δ_{94}, αS-$C^{Bdp}{}_{42}$, and αS-$C^{Bdp}{}_{42}\delta_{94}$ fibrils were diluted to a final concentration of 10 μM (relative to αS monomer) into 1× PBS buffer and pipetted in triplicate into nonsterile Greiner black, flat μClear, 96 well half area microplates to a final volume of 100 μL. Additionally, BODIPY acid (see Appendix S1 for synthesis), Acd amino acid, αS-$C^{Bdp}{}_{42}$, αS-δ_{94}, and αS-$C^{Bdp}{}_{42}\delta_{94}$ monomer were all diluted to 0.5 μM to act as controls. Prior to small molecule addition, fluorescence intensity values were obtained for each construct to optimize gain and Z-position using $\lambda_{ex} = 410 \pm 5$ nm and reading at $\lambda_{em} = 515 \pm 5$ nm. Additionally, gain and z-position were optimized for direct excitation of each fluorophore. Acd: $\lambda_{ex} = 385 \pm 5$ nm, $\lambda_{em} = 420 \pm 5$ nm; BODIPY: $\lambda_{ex} = 490 \pm 5$ nm, $\lambda_{em} = 515 \pm 5$ nm. Initial ($t = 0$ h) emission scans were obtained for each construct prior to small molecule addition, exciting at $\lambda_{ex} = 410 \pm 5$ nm, scanning from $\lambda_{em} = 425$ to 600 ± 5 nm, in 1 nm increments, with a 40 μs integration time. Small molecules were then added to a final concentration of 100 μM. The plates were then covered with an anti-evaporation guard and incubated at 37°C with shaking at 500 rpm. Measurements were taken using the same parameters at 1, 3, and 24 h after small molecule addition. FRET data analysis is described in detail in Appendix S1.

4.5 | LexA/RecA fluorescence anisotropy experiments

Kinetic fluorescence anisotropy experiments were performed on a KinTek SF-120 stopped-flow and collected data was globally fit as described in previous work (Hostetler et al., 2020; Cory et al., 2022a). Endpoint equilibrium data was also collected and analyzed as previously described (Coelho-Cerqueira et al., 2014).

4.6 | LexA/RecA FRET experiments

Reactions were prepared in a final volume of 140 μL with the following concentration of components: [RecA] = 6 μM, [LexA] = 500 nM, and [ssDNA/$ssDNA^{Bdp}$] = 500 nM. A blank sample was prepared by mixing the storage buffers of each component at the same ratios to produce a buffer-matched sample lacking any label, protein, or nucleic acid. In order to control complex formation, ATPγS was either included (SOS complex formation) or excluded (unbound components). These controls allowed for background correction of the traces and a quantitative readout of direct excitation of either fluorophore. Each sample was read on a Photon Technology International (PTI) QuantaMaster™ 40 fluorescence spectrometer with first $\lambda_{ex} = 385$ nm and $\lambda_{em} = 400$–600 nm to measure FRET between Acd and BODIPY followed by $\lambda_{ex} = 490$ nm and $\lambda_{em} = 500$–600 nm to measure direct excitation of BODIPY. Because of the solvatochromic effects experienced by each fluorophore independent of FRET, to obtain a "baseline" signal we combined the measured, background corrected signal from a sample containing only $ssDNA^{Bdp}$ and RecA (RecA* Bdp) and the measured, background corrected signal obtained from a sample containing RecA, unlabeled oligo, and LexA-δ_{161} (SOS complex δ). FRET data analysis is described in detail in Appendix S1.

AUTHOR CONTRIBUTIONS

Michael Cory: Conceptualization (lead); investigation (lead); writing – original draft (lead); writing – review and editing (lead). **Chloe Jones:** Conceptualization (lead); investigation (lead); writing – original draft (supporting); writing – review and editing (supporting). **Kyle Shaffer:** Formal analysis (supporting); investigation (lead); writing – original draft (supporting). **Yarra Venkatesh:** Investigation (supporting); resources (supporting); writing – original draft (supporting). **Sam Giannakoulias:** Software (supporting); visualization (supporting); writing – review and editing (supporting). **Ryann Perez:** Investigation (supporting); writing – review and editing (supporting). **Marshall Lougee:** Investigation (supporting); writing – review and editing (supporting). **Vinayak Pagar:** Investigation (supporting); resources (supporting); writing – review and editing (supporting). **Eshe Hummingbird:** Investigation (supporting); writing – review and editing (supporting). **Christina Hurley:** Investigation (supporting); resources (supporting); writing – review and editing (supporting). **Allen Li:** Investigation (supporting); resources (supporting); writing – review and editing (supporting). **Robert Mach:** Funding acquisition (supporting); supervision (supporting); writing – review and editing (supporting). **Rahul Kohli:** Conceptualization (supporting); funding acquisition (supporting); writing – original draft (supporting); writing – review and editing (supporting). **E. James Petersson:** Conceptualization (lead); funding acquisition (lead); writing – original draft (lead); writing – review and editing (lead).

ACKNOWLEDGMENTS

This research was funded by the University of Pennsylvania and by the National Institutes of Health (NIH R01-NS103873 to E. James Petersson supporting αS FRET studies, NIH U19-NS110456 to E. James Petersson and Robert H. Mach supporting αS PET tracer development, R01-GM127593 to Rahul M. Kohli and E. James Petersson supporting LexA/RecA studies). Marshall G. Lougee was supported by an Age Related Neurodegenerative Disease Training Grant fellowship (NIH T32-AG000255). Chloe M. Jones, Christina M. Hurley, and Ryann M. Perez were supported by the NIH Chemistry Biology Interface Training Program (T32-GM071399 and T32-GM133398). Sam Giannakoulias thanks the National Science Foundation for funding through the Graduate Research Fellowship Program (DGE-1845298). Instruments supported by the NIH and NSF include NMR (NSF CHE-1827457) and mass spectrometers (NIH S10-OD030460).

DATA AVAILABILITY STATEMENT

The data that support the findings of this study are available from the corresponding author upon reasonable request.

ORCID

E. James Petersson https://orcid.org/0000-0003-3854-9210

REFERENCES

Adikesavan AK, Katsonis P, Marciano DC, Lua R, Herman C, Lichtarge O. Separation of recombination and SOS response in Escherichia coli RecA suggests LexA interaction sites. PLoS Genet. 2011;7:e1002244.

Afitska K, Fucikova A, Shvadchak VV, Yushchenko DA. Modification of C terminus provides new insights into the mechanism of alpha-Synuclein aggregation. Biophys J. 2017;113:2182–91.

Aliyan A, Cook NP, Martí AA. Interrogating amyloid aggregates using fluorescent probes. Chem Rev. 2019;119:11819–56.

Batjargal S, Walters CR, Petersson EJ. Inteins as traceless purification tags for unnatural amino acid proteins. J Am Chem Soc. 2015;137:1734–7.

Bell JC, Kowalczykowski SC. RecA: regulation and mechanism of a molecular search engine. Trends Biochem Sci. 2016;41:491–507.

Benskey MJ, Perez RG, Manfredsson FP. The contribution of alpha synuclein to neuronal survival and function – implications for Parkinson's disease. J Neurochem. 2016;137:331–59.

Bünzli J-CG, Eliseeva SV. Basics of lanthanide photophysics. In: Hänninen P, Härmä H, editors. Lanthanide luminescence: photophysical, analytical and biological aspects. Berlin Heidelberg, Berlin, Heidelberg: Springer; 2011. p. 1–45.

Butala M, Klose D, Hodnik V, Rems A, Podlesek Z, Klare JP, et al. Interconversion between bound and free conformations of LexA orchestrates the bacterial SOS response. Nucleic Acids Res. 2011;39:6546–57.

Chen X, Levine L, Kwok P-Y. Fluorescence polarization in homogeneous nucleic acid analysis. Genome Res. 1999;9:492–8.

Chen Z, Yang H, Pavletich NP. Mechanism of homologous recombination from the RecA–ssDNA/dsDNA structures. Nature. 2008;453:489–94.

Cheng Z, Kuru E, Sachdeva A, Vendrell M. Fluorescent amino acids as versatile building blocks for chemical biology. Nat Rev Chem. 2020;4:275–90.

Coelho-Cerqueira E, Pinheiro AS, Follmer C. Pitfalls associated with the use of Thioflavin-T to monitor anti-fibrillogenic activity. Bioorg Med Chem Lett. 2014;24:3194–8.

Cory MB, Hostetler ZM, Kohli RM. Chapter seven – kinetic dissection of macromolecular complex formation with minimally perturbing fluorescent probes. In: Carlson EE, editor. Methods in enzymology. Cambridge, Massachusetts: Academic Press; 2022a. p. 151–71.

Cory MB, Li A, Hurley CM, Hostetler ZM, Venkatesh Y, Jones CM, et al. Engineered RecA constructs reveal the minimal SOS activation complex. Biochemistry. 2022b;61:2884–96.

Culyba MJ, Kubiak JM, Mo CY, Goulian M, Kohli RM. Non-equilibrium repressor binding kinetics link DNA damage dose to transcriptional timing within the SOS gene network. PLoS Genet. 2018;14:e1007405.

Culyba MJ, Mo CY, Kohli RM. Targets for combating the evolution of acquired antibiotic resistance. Biochemistry. 2015;54:3573–82.

Dadabhoy A, Faulkner S, Sammes PG. Long wavelength sensitizers for europium(iii) luminescence based on acridone derivatives. J Chem Soc Perkin Trans. 2002;2:348–57.

Daniels MJ, Nourse JB, Kim H, Sainati V, Schiavina M, Murrali MG, et al. Cyclized NDGA modifies dynamic α-synuclein monomers preventing aggregation and toxicity. Sci Rep. 2019;9:2937.

Ferrie JJ, Ieda N, Haney CM, Walters CR, Sungwienwong I, Yoon J, et al. Multicolor protein FRET with tryptophan, selective coumarin-cysteine labeling, and genetic acridonylalanine encoding. Chem Commun (Camb). 2017;53:11072–5.

Ferrie JJ, Lengyel-Zhand Z, Janssen B, Lougee MG, Giannakoulias S, Hsieh C-J, et al. Identification of a nanomolar affinity α-synuclein fibril imaging probe by ultra-high throughput in silico screening. Chem Sci. 2020;11:12746–54.

Gao B, Liang L, Su L, Wen A, Zhou C, Feng Y. Structural basis for regulation of SOS response in bacteria. Proc Natl Acad Sci. 2023;120:e2217493120.

Giannakoulias S, Shringari SR, Ferrie JJ, Petersson EJ. Biomolecular simulation based machine learning models accurately predict sites of tolerability to the unnatural amino acid acridonylalanine. Sci Rep. 2021;11:18406.

Giese KC, Michalowski CB, Little JW. RecA-dependent cleavage of LexA dimers. J Mol Biol. 2008;377:148–61.

Guerrero-Ferreira R, Taylor NMI, Mona D, Ringler P, Lauer ME, Riek R, et al. Cryo-EM structure of alpha-synuclein fibrils. Elife. 2018;7.

Haas E. The study of protein folding and dynamics by determination of intramolecular distance distributions and their fluctuations using ensemble and single-molecule FRET measurements. ChemPhysChem. 2005;6:858–70.

Haney CM, Cleveland CL, Wissner RF, Owei L, Robustelli J, Daniels MJ, et al. Site-specific fluorescence polarization for studying the disaggregation of α-synuclein fibrils by small molecules. Biochemistry. 2017;56:683–91.

Haney CM, Petersson EJ. Fluorescence spectroscopy reveals N-terminal order in fibrillar forms of α-synuclein. Chem Commun. 2018;54:833–6.

Haney CM, Wissner RF, Petersson EJ. Multiply labeling proteins for studies of folding and stability. Curr Opin Chem Biol. 2015;28:123–30.

Haney CM, Wissner RF, Warner JB, Wang YJ, Ferrie JJ, Covell DJ, et al. Comparison of strategies for non-perturbing labeling of alpha-synuclein to study amyloidogenesis. Org Biomol Chem. 2016;14:1584–92.

Hostetler ZM, Cory MB, Jones CM, Petersson EJ, Kohli RM. The kinetic and molecular basis for the interaction of LexA and activated RecA revealed by a fluorescent amino acid probe. ACS Chem Biol. 2020;15:1127–33.

Hostetler ZM, Ferrie JJ, Bornstein MR, Sungwienwong I, Petersson EJ, Kohli RM. Systematic evaluation of soluble protein expression using a fluorescent unnatural amino acid reveals no reliable predictors of tolerability. ACS Chem Biol. 2018;13:2855–61.

Hsieh C-J, Ferrie JJ, Xu K, Lee I, Graham TJA, Tu Z, et al. Alpha synuclein fibrils contain multiple binding sites for small molecules. ACS Chem Nerosci. 2018;9:2521–7.

Jones CM, Robkis DM, Blizzard RJ, Munari M, Venkatesh Y, Mihaila TS, et al. Genetic encoding of a highly photostable, long lifetime fluorescent amino acid for imaging in mammalian cells. Chem Sci. 2021;12:11955–64.

Jones CM, Venkatesh Y, Petersson EJ. Chapter three – protein labeling for FRET with methoxycoumarin and acridonylalanine. In: Chenoweth DM, editor. Methods in enzymology. Cambridge, Massachusetts: Academic Press; 2020. p. 37–69.

Karpowicz RJ Jr, Haney CM, Mihaila TS, Sandler RM, Petersson EJ, Lee VMY. Selective imaging of internalized proteopathic α-synuclein seeds in primary neurons reveals mechanistic insight into transmission of synucleinopathies. J Biol Chem. 2017;292:13482–97.

Kitada S, Leone M, Sareth S, Zhai D, Reed JC, Pellecchia M. Discovery, characterization, and structure−activity relationships studies of proapoptotic polyphenols targeting B-cell lymphocyte/Leukemia-2 proteins. J Med Chem. 2003;46:4259–64.

Koga S, Sekiya H, Kondru N, Ross OA, Dickson DW. Neuropathology and molecular diagnosis of synucleinopathies. Mol Neurodegen. 2021;16:83.

Korat Š, Bidesi NS, Bonanno F, Di Nanni A, Hoàng AN, Herfert K, et al. Alpha-synuclein PET tracer development—an overview about current efforts. Pharmaceuticals. 2021;14(9):847.

Kovačič L, Paulič N, Leonardi A, Hodnik V, Anderluh G, Podlesek Z, et al. Structural insight into LexA–RecA* interaction. Nucleic Acids Res. 2013;41:9901–10.

Kuimova MK. Mapping viscosity in cells using molecular rotors. Phys Chem Chem Phys. 2012;14:12671–86.

Lakowicz J. 2006. Principles of fluorescence spectroscopy, New York, NY: Springer.

Lengyel-Zhand Z, Ferrie JJ, Janssen B, Hsieh C-J, Graham T, Xu K-y, et al. Synthesis and characterization of high affinity fluorogenic α-synuclein probes. Chem Commun. 2020;56:3567–70.

Little JW, Kim B, Roland KL, Smith MH, Lin L-L, Slilaty SN. [20] Cleavage of LexA repressor. Methods in enzymology. Cambridge, Massachusetts: Academic Press; 1994. p. 266–84.

Lougee MG, Pagar VV, Kim HJ, Pancoe SX, Chia WK, Mach RH, et al. Harnessing the intrinsic photochemistry of isoxazoles for the development of chemoproteomic crosslinking methods. Chem Commun. 2022;58:9116–9.

Luo Y, Pfuetzner RA, Mosimann S, Paetzel M, Frey EA, Cherney M, et al. Crystal structure of LexA: a conformational switch for regulation of self-cleavage. Cell. 2001;106:585–94.

Marotta NP, Ara J, Uemura N, Lougee MG, Meymand ES, Zhang B, et al. Alpha-synuclein from patient Lewy bodies exhibits distinct pathological activity that can be propagated in vitro. Acta Neuropathol Commun. 2021;9:188.

Maslowska KH, Makiela-Dzbenska K, Fijalkowska IJ. The SOS system: a complex and tightly regulated response to DNA damage. Environ Mol Mutagen. 2019;60:368–84.

Mehra S, Sahay S, Maji SK. Alpha-synuclein misfolding and aggregation: implications in Parkinson's disease pathogenesis. Biochim Biophys Acta Proteins Proteom. 2019;1867:890–908.

Memar MY, Yekani M, Celenza G, Poortahmasebi V, Naghili B, Bellio P, et al. The central role of the SOS DNA repair system in antibiotics resistance: a new target for a new infectious treatment strategy. Life Sci. 2020;262:118562.

Pancoe SX, Wang YJ, Shimogawa M, Perez RM, Giannakoulias S, Petersson EJ. Effects of mutations and post-translational

modifications on α-synuclein in vitro aggregation. J Mol Biol. 2022;434:167859.
Park SH, Raines RT. Fluorescence polarization assay to quantify protein-protein interactions. Methods Mol Biol. 2004;261: 161–6.
Peelaerts W, Bousset L, Van der Perren A, Moskalyuk A, Pulizzi R, Giugliano M, et al. α-Synuclein strains cause distinct synucleinopathies after local and systemic administration. Nature. 2015;522:340–4.
Peng C, Gathagan RJ, Covell DJ, Medellin C, Stieber A, Robinson JL, et al. Cellular milieu imparts distinct pathological α-synuclein strains in α-synucleinopathies. Nature. 2018;557: 558–63.
Podlesek Z, Žgur Bertok D. The DNA damage inducible SOS response is a key player in the generation of bacterial persister cells and population wide tolerance. Front Microbiol. 2020;11.
Qiao Y, Luo Y, Long N, Xing Y, Tu J. Single-molecular Forster resonance energy transfer measurement on structures and interactions of biomolecules. Micromachines (Basel). 2021;12(5):492.
Rajan R, Wisler JW, Bell CE. Probing the DNA sequence specificity of Escherichia coli RECA protein. Nucleic Acids Res. 2006;34:2463–71.
Reynolds AM, Sculimbrene BR, Imperiali B. Lanthanide-binding tags with unnatural amino acids: sensitizing Tb3+ and Eu3+ luminescence at longer wavelengths. Bioconjug Chem. 2008;19: 588–91.
Rossi AM, Taylor CW. Analysis of protein-ligand interactions by fluorescence polarization. Nat Protoc. 2011;6:365–87.
Schuler B, Eaton WA. Protein folding studied by single-molecule FRET. Curr Opin Struct Biol. 2008;18:16–26.
Schulz-Schaeffer WJ. The synaptic pathology of alpha-synuclein aggregation in dementia with Lewy bodies, Parkinson's disease and Parkinson's disease dementia. Acta Neuropathol. 2010;120: 131–43.
Sletten EM, Bertozzi CR. Bioorthogonal chemistry: fishing for selectivity in a sea of functionality. Angew Chem Int Ed. 2009;48: 6974–98.
Slilaty SN, Little JW. Lysine-156 and serine-119 are required for LexA repressor cleavage: a possible mechanism. Proc Natl Acad Sci. 1987;84:3987–91.
Slilaty SN, Rupley JA, Little JW. Intramolecular cleavage of lexA and phage lambda repressors: dependence of kinetics on repressor concentration, pH, temperature, and solvent. Biochemistry. 1986;25:6866–75.
Speight LC, Muthusamy AK, Goldberg JM, Warner JB, Wissner RF, Willi TS, et al. Efficient synthesis and in vivo incorporation of Acridon-2-ylalanine, a fluorescent amino acid for lifetime and Förster resonance energy transfer/luminescence resonance energy transfer studies. J Am Chem Soc. 2013;135:18806–14.
Speight LC, Samanta M, Petersson EJ. Minimalist approaches to protein labelling: getting the most fluorescent bang for your steric Buck. Aust J Chem. 2014;67:686–700.
Stryer L, Haugland RP. Energy transfer – a spectroscopic ruler. Proc Natl Acad Sci USA. 1967;58:719–26.
Sungwienwong I, Ferrie JJ, Jun JV, Liu C, Barrett TM, Hostetler ZM, et al. Improving the fluorescent probe acridonylalanine through a combination of theory and experiment. J Phys Org Chem. 2018;31.
Sungwienwong I, Hostetler ZM, Blizzard RJ, Porter JJ, Driggers CM, Mbengi LZ, et al. Improving target amino acid selectivity in a permissive aminoacyl tRNA synthetase through counter-selection. Org Biomol Chem. 2017;15:3603–10.
Tanaka T, Wagner AM, Warner JB, Wang YJ, Petersson EJ. Expressed protein ligation at methionine: N-terminal attachment of homocysteine, ligation, and masking. Angew Chem Int Ed. 2013;52:6210–3.
Tuttle MD, Comellas G, Nieuwkoop AJ, Covell DJ, Berthold DA, Kloepper KD, et al. Solid-state NMR structure of a pathogenic fibril of full-length human alpha-synuclein. Nat Struct Mol Biol. 2016;23:409–15.
Van Der Meer BW, Coker G III, Chen S-YS. Resonance energy transfer. New York, NY: VCH Publishers, Inc; 1994.
VanEngelenburg SB, Palmer AE. Fluorescent biosensors of protein function. Curr Opin Chem Biol. 2008;12:60–5.
VanLoock MS, Yu X, Yang S, Galkin VE, Huang H, Rajan SS, et al. Complexes of RecA with LexA and RecX differentiate between active and inactive RecA nucleoprotein filaments. J Mol Biol. 2003;333:345–54.
Wu PG, Brand L. Resonance energy-transfer – methods and applications. Anal Biochem. 1994;218(1):1–13.
Yoon J, Ferrie JJ, Petersson EJ. Improved modeling of thioamide FRET quenching by including conformational restriction and coulomb coupling. J Phys Chem B. 2020;124:10653–62.
Yu X, Egelman EH. The LexA repressor binds within the deep helical groove of the activated RecA filament. J Mol Biol. 1993;231: 29–40.
Zagotta WN, Sim BS, Nhim AK, Raza MM, Evans EG, Venkatesh Y, et al. An improved fluorescent noncanonical amino acid for measuring conformational distributions using time-resolved transition metal ion FRET. Elife. 2021;10.

SUPPORTING INFORMATION

Additional supporting information can be found online in the Supporting Information section at the end of this article.

How to cite this article: Cory MB, Jones CM, Shaffer KD, Venkatesh Y, Giannakoulias S, Perez RM, et al. FRETing about the details: Case studies in the use of a genetically encoded fluorescent amino acid for distance-dependent energy transfer. Protein Science. 2023;32(5):e4633. https://doi.org/10.1002/pro.4633